Enzyme and Microbial Technology 45 (2009) 274–281

Contents lists available at ScienceDirect

Enzyme and Microbial Technology

journal homepage: www.elsevier.com/locate/emt

Visualization of enzymatic hydrolysis of cellulose using AFM phase imaging

Hao Liu [a,*], Shiyu Fu [a], J.Y. Zhu [b], Hui Li [a], Huaiyu Zhan [a]

[a] State Key Laboratory of Pulp and Paper Engineering, South China University of Technology, Guangzhou 510640, China
[b] U.S. Forest Service, Forest Products Laboratory, Madison, WI 53726, USA

ARTICLE INFO

Article history:
Received 19 February 2009
Received in revised form 5 June 2009
Accepted 8 June 2009

Keywords:
Ultrastructure
Cellulose
Enzymatic hydrolysis
Cellulases
Microfibrils
Atomic force microscopy (AFM)
Phase imaging
Endoglucanase (EG)
Cellulose-binding domain (CBD)

ABSTRACT

Complete cellulase, an endoglucanase (EGV) with cellulose-binding domain (CBD) and a mutant endoglucanase without CBD (EGI) were utilized for the hydrolysis of a fully bleached reed Kraft pulp sample. The changes of microfibrils on the fiber surface were examined with tapping mode atomic force microscopy (TM–AFM) phase imaging. The results indicated that complete cellulase could either peel the fibrillar bundles along the microfibrils (peeling) or cut microfibrils into short length across the length direction (cutting) during the process. After 24 h treatment, most orientated microfibrils on the cellulose fiber surface were degraded into fragments by the complete cellulase. Incubation with endoglucanase (EGV or EGI) also caused peeling action. But no significant size reduction of microfibrils length was observed, which was probably due to the absence of cellobiohydrolase. The AFM phase imaging clearly revealed that individual EGV particles were adsorbed onto the surface of a cellulose fiber and may be bound to several microfibrils.

Published by Elsevier Inc.

1. Introduction

The hydrolysis of native cellulose from plant fibers, such as wood and agricultural residues, is a key step for converting biomass to biofuels through biochemical means [1]. Cellulases are chosen preferentially to cleave β-1,4-glucosidic linkage in polysaccharide chains and thus completely hydrolyze cellulose to glucose [2]. The widely accepted mechanism suggests that three functionally different types of enzymes work together synergistically in a complete cellulase system during such a process [3,4]. β-1,4-endoglucanases (EG, EC 3.2.1.4) have been shown to randomly attack accessible intramolecular β-1,4-glucosidic bonds in cellulosic substrates, producing new chain ends and rapidly decreasing the cellulose chain length, whereas β-1,4-cellobiohydrolases (CBH, EC 3.2.1.91) progressively release soluble cellobiose from the end of cellulose chains [2]. The EG–CBH synergistic action can be generally explained by the EG generating new free chain ends for the CBH to act upon [5,6]. Another individual cellulase, β-glucosidase (BGL, EC 3.2.1.21), subsequently cleaves cellobiose to glucose, which eliminates the inhibition caused by the accumulating cellobiose [2,4].

Cellulose exists in the form of microfibrils with an unknown length in the plant cell wall, rather than free glucan chains [7–9]. The ultrastructure of microfibrils (diameter 10–30 nm) was regarded as an assembled organization of a core crystalline region and surrounded by paracrystalline regions, often called elementary fibrils (diameter approximately 3.5 nm) [8]. Mühlethaler [9] proposed that an elementary fibril was the smallest cellulosic strand, comprised of about 36 hydrogen-bonded chains of β-1, 4-glucose. To understand the process of enzymatic hydrolysis of cellulose, it is necessary to directly investigate and visualize the degradation or modification of microfibrils by cellulases through the combined actions and synergistic effects of EG, CBH, and BGL.

Electron microscopy has been used frequently to visualize the ultrastructure of cellulose microfibrils as well as the bound cellulases [7,10–12]. Nevertheless, this technique cannot provide detailed 3-dimensional information, such as height and roughness [11]. Many efforts have been made to observe the surface topographies of cellulosic substrates by atomic force microscopy (AFM) [12]. AFM can be used to examine samples at molecular or even atomic resolutions in three dimensions. It also has the advantages of in situ measurements in atmospheric or controlled environments without special sample preparation [12]. Tapping mode (TM) AFM, employing a silicon cantilever probe to gently oscillate and tap the sample surface, is suitable for scanning soft materials at low forces [13]. TM–AFM topographical images of enzyme-treated cotton fibers have been reported by Lee et al. [14,15]. They found that incubation with CBH I or EG II caused different effects on fiber surfaces, and the presence of both enzymes produced the greatest effect on cellulose destruction [14].

TM–AFM phase imaging can produce very high material contrast of fine structures that barely can be seen in topographical imaging. The cantilever is excited into resonance oscillation in TM–AFM.

* Corresponding author.
E-mail address: laccase2008@yahoo.com.cn (H. Liu).

0141-0229/$ – see front matter. Published by Elsevier Inc.
doi:10.1016/j.enzmictec.2009.06.009

With the presence of surface viscous damping, or adhesion such as hydrophilic attraction, the shift in the phase of the oscillation reflects the variation in substrate surface stiffness [16]. Any boundaries with material discontinuity caused by the difference in surface properties can be reflected by phase shift. Therefore, AFM phase imaging is very effective for visualizing microfibril surface features such as edges, damages, and breakage, or fragmentations and contaminants. Under light tapping force conditions, the tip cannot penetrate the water film that exists on a hydrophilic surface. The tip responds to hydrophilic interactions with the substrate surface. Therefore, an AFM phase image can differentiate materials with different hydrophilicity [17,18]. With this method, Simola et al. [17] and Chernoff [19] used phase imaging to show microfibrils and fine lignin structure on wood fiber surfaces. However, few studies reported visualizing the binding of endoglucanase particles to lignocellulose through CBD using AFM phase imaging.

Several approaches visualize cellulase particles binding onto cellulose substrates directly, such as scanning electron microscopy (SEM), transmission electron microscopy (TEM), and quantitative fluorescence microscopy (QFM) [20–22]. Compared with these techniques, TM–AFM produces sharper images to distinguish enzyme particles from cellulose microfibrils or fragments. As discussed above, distinct features of materials (hard or soft, hydrophobic or hydrophilic) can be revealed using AFM phase imaging.

In this study, we used moderate tapping force mode to produce an AFM phase image to visualize the fragmentation of cellulose microfibrils from enzymatic hydrolysis based on the discontinuity of material surface mechanical properties. We are focused on the study of the effect of endoglucanase with (EGV) or without (EGI) a cellulose-binding domain (CBD), on the ultrastructure of cellulose microfibrils of reed Kraft pulp fibers. We also used the light tapping force mode to produce an AFM phase image to visualize the binding of enzymes onto microfibrils based on the difference in the hydrophilicity between microfibrils and enzymes. The images revealed significant differences between EGV binding and EGI adsorption onto microfibrils at a nanoscale.

2. Experimental

2.1. Cellulosic substrate

A reed Kraft pulp was bleached by an O–LMS–E–X–Q–P bleaching sequence under optimum conditions as described by Fu et al. [23] and Zhan et al. [24]. This sequence consists of an oxygen delignification (O), a laccase mediator treatment (LMS), an alkaline extraction (E), a xylanase treatment (X), and a peroxide bleaching process (Q–P). The final bleached pulp reached 88.2% ISO brightness with kappa number 0.4 and viscosity 705 $cm^3\ g^{-1}$ determined by TAPPI standard methods [25]. The cellulose content was 82.2% using HPLC with refraction index detection after acid hydrolysis. The yield of monomeric hemicellulose sugars from the pulp sample was about 9%.

2.2. Enzymes

Three different commercial cellulases (Table 1) were purchased from Novozymes (Bagsvaerd, Denmark). Novozym 342 (N342) is a multicomponent cellulase preparation (or called complete cellulase) containing endoglucanase, exoglucanase, and β-glucosidase. Novozym 476 (N476) is a monocomponent endoglucanase (EGV) with a CBD, whereas Novozym 613 (N613) is a monocomponent endoglucanase (EGI) without a CBD. The activities of the cellulases preparations were determined according to the International Union of Pure and Applied Chemistry-recommended procedures [26].

2.3. Enzymatic hydrolysis

The enzymatic treatments were carried out in a shaking water bath (150 rpm) at 50 °C at a substrate consistency of 1% (w/v). Separate hydrolysis experiments were conducted using different cellulases. An enzyme loading of 5 FPU per gram oven-dried pulp was applied in all experiments. An acetate buffer (0.1 mol/L, pH 5.0) was used to maintain the pH at 5.0 ± 0.1. After incubation, each substrate was washed thoroughly using dilute NaOH solution of concentration 10 mM and Milli-Q water, and then centrifuged to remove the liquor. To observe enzyme particles, the substrates incubated with EGI and EGV were washed with acetate buffer one time following centrifugation.

2.4. Analysis of hydrolysates

The total amount of soluble-reducing sugars released in the hydrolysates was determined by the DNS method [27] using glucose as the standard. The soluble-reducing sugar yield is the amount of reducing sugar measured in weight percent of the pulp sample. The measured reducing sugar yield and dry weight loss of the substrate were used to represent the cellulose conversion efficiency. Data were collected at different incubation duration times of 2, 4, 6, 12, and 24 h.

2.5. Atomic force microscopy (AFM)

The samples for AFM were prepared as follows: first, a piece of freshly cleaved mica (Veeco, Santa Barbara, CA, US) was attached onto an iron stub with an adhesive tab; then about 0.2 ml fiber suspension (0.1 g pulp in 100 ml Milli-Q water) was dropped onto the mica surface; finally, the sample was dried in a vacuum desiccator for 24 h. To ensure that the AFM images obtained were representative, AFM scanning was conducted at two to four locations on each fiber characterized. Two fibers were characterized on each of two micas prepared. Therefore, a total of 8–16 locations were imaged for each sample. For each imaging location, duplicate scans were conducted at each location.

A commercial Multimode Nanoscope IIIa AFM system (Veeco, Santa Barbara, CA, US) was used to study the surface characteristics of cellulose fibers. The AFM system was equipped with an E-type scanner and a standard silicon cantilever (Veeco model No. RTESP) with a length of 125 μm. The spring constant of the cantilever is 20 N/m. The tip radius is less than 10 nm based on manufacture specification. All images were obtained using the tapping mode in air at room temperature with relative humidity lower than 5%. Real time scanning was performed with scan rates 1.0 Hz, scan angle 0°, and tapping frequencies ranging from 290 to 320 kHz. Tapping force was controlled by the ratio between setpoint amplitude (A_{sp}) and free-air amplitude (A_0). Light tapping force ($A_{sp}/A_0 = 0.7–0.8$) was applied to examining enzyme particles bound onto microfibrils. Moderate tapping force ($A_{sp}/A_0 = 0.5–0.6$) was used for the remaining imaging experiments. Both topographical and phase images were captured for each sample. For offline image flattening and analysis, the software Nanoscope III 5.12r3 was used.

3. Results and discussions

3.1. Cellulose bioconversion

The enzymatic conversion of cellulose substrates by 3 different cellulases is shown in Table 2. After incubation with complete cellulase (N342) for 24 h, an enzymatic hydrolysis-reducing sugar yield was 22.6%. However, nearly 49% of the substrate's dry weight was lost (Table 2), which suggests that many soluble oligosaccharides were formed but not converted into glucose. For the substrate hydrolyzed by N342, samples after 6, 12, and 24 h of hydrolysis were selected for AFM examination to demonstrate the present AFM visualization technique.

Individual endoglucanase (EGV and EGI) produced very low cellulose conversion after 24 h incubation, as can be seen from the measured soluble-reducing sugar yield, <1.3%, from Table 2. Dry weight losses were 12.5% and 5.9% (Table 2), significantly greater than 1.3%. Apparently, endoglucanase is only able to break down microfibrils into small particles, or called "fragments". Because this

Table 1
The characteristics of the three cellulases used in this study.

Commercial enzyme	Component	Origin	CBD	FPase activity (IU/ml)	CMCase activity (IU/ml)
Novozym 342	EG, CBH, BGL	*Humicola insolens*	–	20.3	84.6
Novozym 476	EGV	*Humicola* spp.	Yes	17.6	67.5
Novozym 613	EGI	Genetically modified *Aspergillus* spp.	No	10.9	55.2

Table 2
Time-dependent soluble-reducing sugar yields and dry weight losses of the bleached reed kraft pulp hydrolyzed by different cellulases (the errors listed below are from duplicate measurements).

Incubation time (h)	Soluble-reducing sugar yield (wt% dry solid)			Dry weight loss (%)		
	N342	N476	N613	N342	N476	N613
2	7.2 ± 0.7	1.0 ± 0.0	0.8 ± 0.0	20.2 ± 2.1	3.5 ± 0.1	3.4 ± 0.2
4	10.2 ± 0.4	1.1 ± 0.1	0.9 ± 0.1	25.4 ± 1.6	4.8 ± 0.1	3.6 ± 0.3
6	12.8 ± 2.2	1.1 ± 0.0	1.0 ± 0.0	30.5 ± 1.0	5.5 ± 0.3	4.8 ± 0.3
12	18.9 ± 1.5	1.2 ± 0.1	1.0 ± 0.1	40.2 ± 1.4	8.3 ± 0.3	5.5 ± 0.6
24	22.6 ± 3.0	1.3 ± 0.1	1.1 ± 0.1	49.1 ± 2.2	12.5 ± 0.6	5.9 ± 0.3

fragmentation process is the rate-controlling process in cellulose conversion [2], we used the samples obtained after 24-h incubation with EGV and EGI to visualize the actions of endoglucanase on cellulose in nanoscale.

3.2. The reliability of AFM scanning

The repeatability and accuracy of AFM scanning is critically important to understanding enzyme actions on cellulose in this study because the physical area covered by each AFM scan is very small, on the order of square micrometers. Visual examinations of all the images (total of about 16 scanning) taken from the same sample showed similar features. Duplicate phase images obtained from the same location of the control (without enzyme action) substrate, bleached reed Kraft pulp sample, are shown in Fig. 1a and b to demonstrate the repeatability and reliability of the AFM-imaging experiments. The image shown in Fig. 1a has a larger scanning area of 1.5 μm × 1.5 μm while the image shown in Fig. 1b has a scanning area of 1.0 μm × 1.0 μm. The features of the microfibrils shown in these two images are identical. Fig. 1b is almost like a zoom view of Fig. 1a, suggesting the excellent repeatability of the AFM scanning. The results of a different AFM scanning carried out at a different location of the control substrate sample are also shown (Fig. 2). The morphologies of the microfibrils shown in Figs. 1b and 2a are similar with typical diameters between 20 and 60 nm, and the lengths are longer than the viewing size of the images. These images suggest the AFM scanning was repeatable and can properly represent the sample.

The phase-bearing area probability of a phase image can provide a quantitative measure of the phase distribution. The phase-bearing area probability densities of the three phase images (Figs. 1a, b and 2a) have very similar bimodal distributions as shown in Fig. 3. The phases of the low phase peaks are all at about 20°, whereas the phases of the high phase peaks are all at about 50°. The low phase regions could represent the valleys between microfibrils on a fiber surface, while the high phase regions could represent the surface of microfibrils. The curves in Fig. 3 denoted as Fig. 1a and b (taken from the same location) are almost identical. The observed similarities of the phase-bearing area probability densities can be quantitatively verified by the intensities and the full-width half maximum of both the low- and high-phase peaks of the three curves (Table 3). The only differences are the locations (phases) of the two peaks. As a result, the phase contrast, the difference between the low and high phase peak of Fig. 2a is slightly smaller than those for Fig. 1a and b. This difference may be because the image shown in Fig. 2 was taken from a different location from that of the images shown in Fig. 1a and b. The variations in other characteristics of the bimodal distributions are within the measurement errors, as the variations between Figs. 1a or b and 2a (scans from different locations) are within the differences between Fig. 1a and b (from the same location). These kinds of similarities of the phase-bearing area probability density curves among images taken from the same sample were found to be true for all the samples scanned in this study, suggesting the reliability of the AFM scanning.

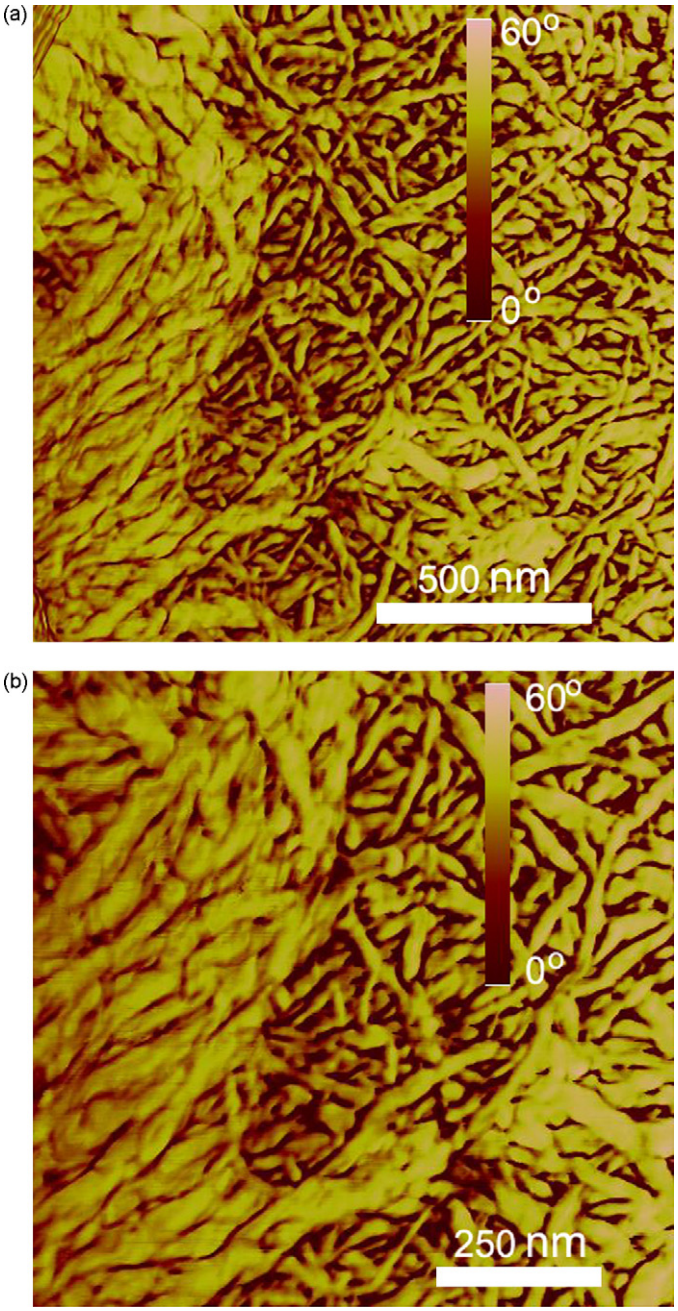

Fig. 1. Atomic force microscopy (AFM) phase images of duplicate scans at the same location of an un-incubated reed kraft pulp fiber: (a) scanning area of 1.5 μm × 1.5 μm, (b) scanning area of 1.0 μm × 1.0 μm.

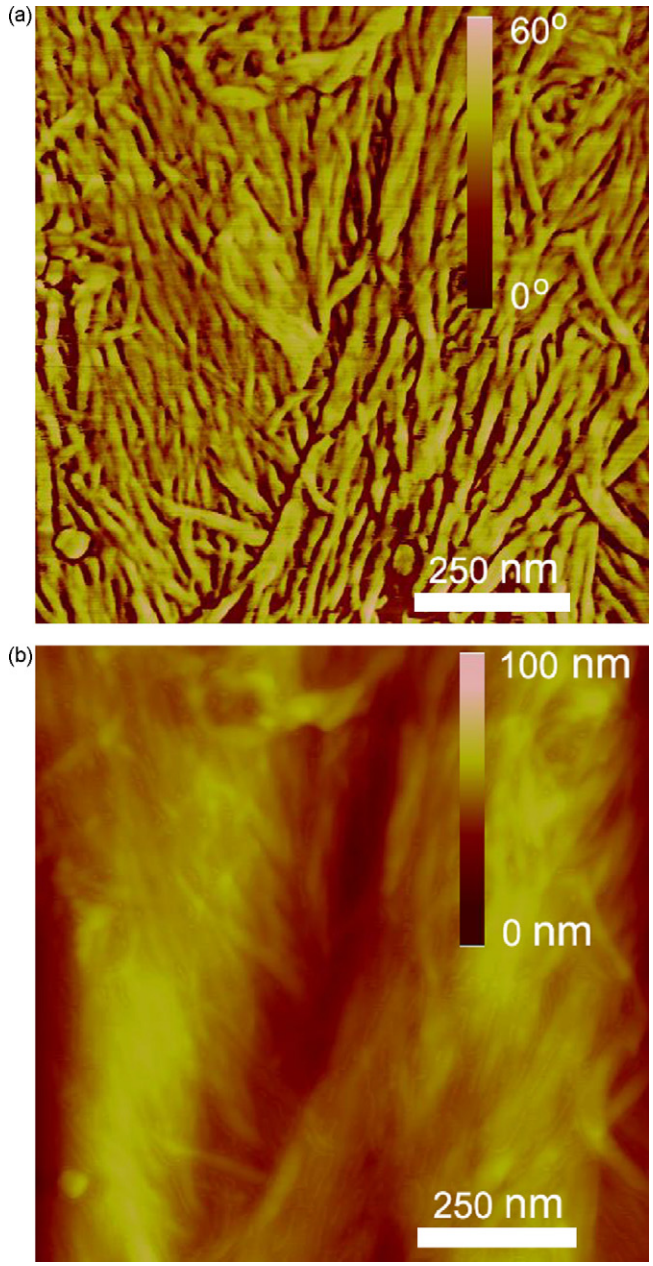

Fig. 2. Atomic force microscopy (AFM) images of a reed kraft pulp fiber: (a) phase image, (b) topographical image.

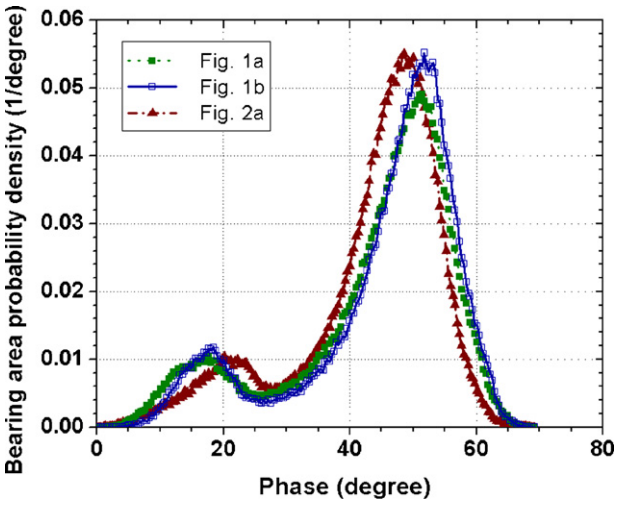

Fig. 3. Phase-bearing-area probability densities of AFM phase images of the control sample of reed kraft pulp shown in Figs. 1a, b and 2a.

3.3. Action of complete cellulase (N342) on microfibrils

The main feature in the phase image of the non-incubated control sample, reed kraft pulp, is microfibrils (Figs. 1a, b and 2a). This feature is very similar to that observed by Simola et al. [17] from an oxygen-delignified wood pulp. The topographical image of Fig. 2a is also shown (Fig. 2b) for comparison. The main structures of the microfibrils are identical in these two images, but the fine structures shown in the phase image (Fig. 2a) cannot be seen in the topographical image (Fig. 2b). Only a couple of particulate-shaped structures with a large phase are seen in Fig. 2a, which is very different from the images obtained from lignin-covered unbleached fibers by Simola et al. [17]. These particulates are not microfibril-like and could be contaminants left over from pulp washing. This observation suggests that bleached reed Kraft pulp fibers are essentially free of lignin or extractives on the surface. The regions with phase at approximately 20° were valleys between microfibrils.

The cellulase complex (N342) was capable of decomposing either amorphous or crystalline regions of the fibers. Significant structural changes of the reed fibers occurred (Fig. 4) upon incubation with complete cellulase N342. After 6 h of exposure to enzymes, the typical morphologies (Fig. 4a) showed that microfibrillar bundles were cut across the microfibril (*x*-axis) direction and peeled along the microfibril (*y*-axis) direction. Lee et al. [14] treated cotton fibers with catalytically inactivated CBH I and found many nanopores. They explained that the nanopores were produced by penetration of CBD into microfibrils. Synergistic activity of CBH and EG makes further degradation of microfibrils possible through enlargement of the nanopores in the directions along (peeling) and across (cutting) the microfibrils.

Table 3
Comparisons of the characteristics of the bimodal distribution of the phase-bearing-area probability density curves shown in Fig. 3.

Curve label	The low phase peak			The high phase peak			Phase contrast (degree)
	Location/phase (degree)	Height/value (1/degree)	FWHM[a] (degree)	Location/phase (degree)	Height/value (1/degree)	FWHM (degree)	
Fig. 1a	18.2	0.0103	13.50	51.2	0.0491	14.33	33.0
Fig. 1b	18.3	0.0117	10.16	51.7	0.0544	13.17	33.4
Fig. 2a	20.2	0.0105	12.83	49.2	0.0547	14.17	29.0
STD[b]	**1.13**	**0.00076**	**1.77**	**1.32**	**0.0032**	**0.63**	**2.43**
RSTD[c] (%)	**5.96**	**6.99**	**14.50**	**2.61**	**5.97**	**4.53**	**7.56**

[a] Full-width half maximum.
[b] Standard deviation.
[c] Relative standard deviation.

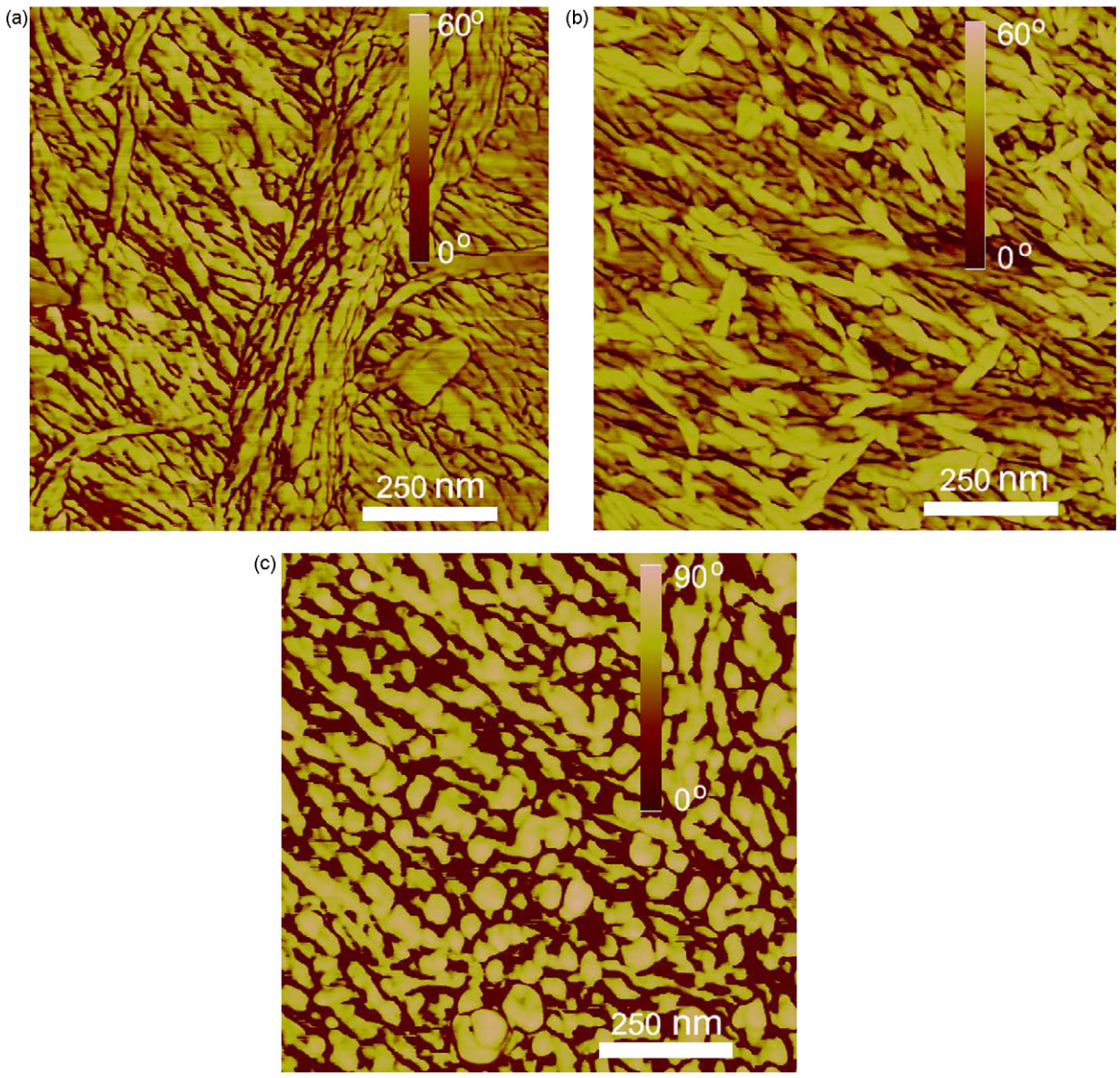

Fig. 4. Atomic force microscopy (AFM) phase images of reed kraft pulp fibers incubated with complete cellulase N342 for different incubation time periods: (a) 6 h; (b) 12 h; (c) 24 h.

After 12 h of reaction, the microfibrils were further degraded into rodlets. The phase image (Fig. 4b) shows that the area of regions with low phase (<20°) or valleys between microfibrils increased, which can be clearly seen from the phase-bearing area probability density plot (Fig. 5). The complete cellulase attacks the amorphous part of the outer microfibrils occurred firstly without significant degradation of the crystalline. The degradation of amorphous cellulose exposed the inner microfibrils, which not only makes the inner microfilbrils accessible to enzymes for further degradation but also produced two layers of surface, the outer crystalline and the inner newly exposed and relatively complete microfibril surface.

After 24 h incubation, almost all the microfibrils were completely fragmented into grain-like particles while some remained rodlet shaped (Fig. 4c). White and Brown [10] regarded these irregular fragments as the final stage of degradation prior to complete solubilization. Phase contrast in Fig. 4c was much higher than that observed in Fig. 4a and b. The images shown (Fig. 4a–c) are more typical of all the phase images obtained from each sample.

We calculated the phase-bearing area probability densities of Figs. 2a and 4a–c to quantitatively examine the effect of enzymatic incubation time on substrate degradation and fragmentation. For the un-incubated sample, the bimodal distribution of the phase-bearing area probability density represents the valleys (around 20°) between microfibrils and the microfibril (around 50°) itself (Fig. 5). After incubation with enzymes for 6 h, the probability densities of the low phases (around 20°) increased and the probability density of the high phases decreased, suggesting that the degradation of the microfibrils reduced the covering area of the microfibrils. Furthermore, the peak of the high phases was up-shifted about 7°, suggesting an increase in surface stiffness perhaps resulted from the degradation of the amorphous region on microfibrils.

After further incubation with enzymes to 12 h, the probability density of the low phases further increased and the peak of the low phases reduced to about 7°, suggesting that the further degradation may have deepened the valleys between microfibrils. Two peaks were observed in the high phases in Fig. 5. Analysis of the phase-bearing area distribution of all the phase images taken from this sample (incubation with enzymes for 12 h) all showed two peaks in the high phases, suggesting that this two-peak feature in the high phases shown in Fig. 5 is not an artifact. The lower peak corresponds to the same phase (around 50°) of the peak as the high phases of the original sample. We believe this peak represents the newly exposed

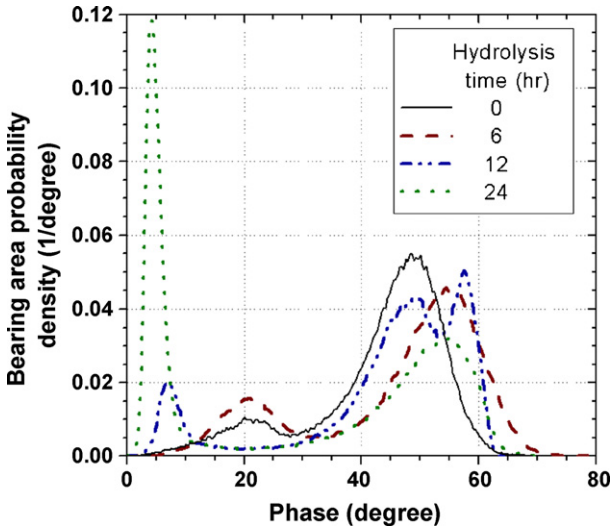

Fig. 5. Phase-bearing-area probability densities of atomic force microscopy (AFM) phase images of the substrate obtained at different enzymatic incubation time periods.

inner microfibrils that had not been subjected to enzyme attack as discussed previously, therefore the phase of this peak should equal to that of the un-incubated microfibrils of 50°. The higher peak was up-shifted about 10°, suggesting an even stiffer surface than that with the sample after 6 h incubation, which may be due to the increase in the crystallinity of the outer remaining micriofibril surface. At the end of 24 h incubation, the probability density of the low phases increased significantly to 0.12; moreover, the peak of the low phase was much more narrow and the phase of the peak was further downshifted to about 4° The probabilities of the intermediate phase were very low and close to zero between 10° and 35°. This suggests that the degradation became much severe and uniform. The physical area of the degraded microfibrils was about 40%. The probability density of the high phases was decreased because of the further reduction of the covering area of the remaining microfibrils.

3.4. Action of endoglucanase EGV or EGI

Endoglucanase is considered to be the most active enzyme in the initial stage of cellulose degradation through breaking glucosidic bonds to weaken microfibrils surface [7,10]. Significant modifications of the ultrastructure of cellulose microfibrils after 24 h incubation by endoglucanase with or without CBD were observed as shown in Fig. 6. Compared with the complete cellulose system shown in Fig. 4, the size reduction of microfibrils in *x* direction (cutting) by the endoglucanases was not as notable as that in *y* direction (peeling). In other words, endoglucanase inclined to modify microfibrils to become thinner (with diameter 5–20 nm) rather than to cut them into fragments. In the absence of CBH, the effectiveness of degrading micorfibrils by endoglucanases was limited by a lack of synergy, as supported by the fact that significant cellulose dry weight loss by the two endoglucanases did not produce soluble-reducing sugars (Table 2).

The microfibrils of the sample treated with EGV showed the sign of damage (Fig. 6a), which was not seen from the sample incubated with EGI (Fig. 6b). Furthermore, endoglucanase EGV (N476) produced more cellulose dry weight loss than EGI (N613) (Table 2). Köpcke's study [28] found that the viscosity of a softwood kraft pulp sample incubated with EGV (N476) was lower than one incubated with EGI (N613), suggesting a lower degree of cellulose polymerization of the sample, This viscosity is the viscosity of the cupriethylenediamine solution dissolved with the pulp sample.

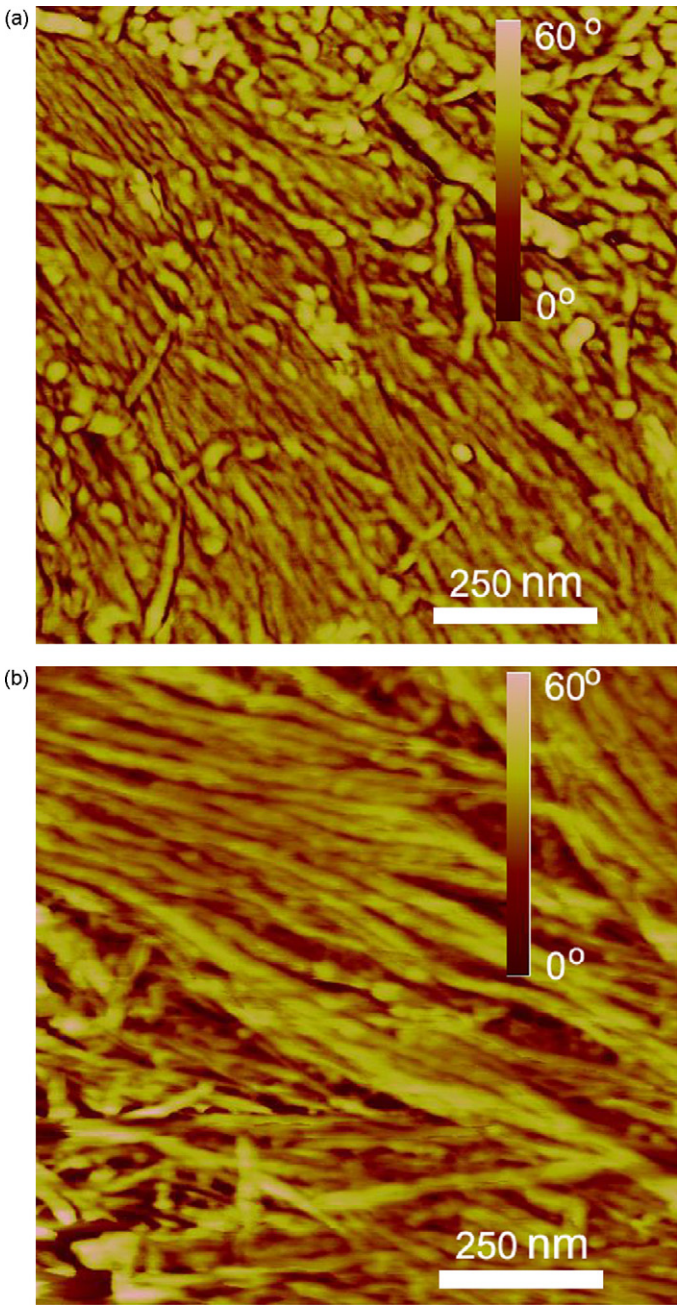

Fig. 6. Atomic force microscopy (AFM) phase images of reed kraft pulp fibers incubated with endoglucanase after 24 h incubation. (a) EGV; (b) EGI.

The differences in dry weight losses and in viscosities suggest that EGV may be more effective in modifying cellulose than EGI, as supported by the AFM phase images (Fig. 6a and b). According to Gilkes et al. [29], CBD in endoglucanases can mediate adsorption to the substrate and thus enhance the hydrolysis of insoluble amorphous cellulose. The absence of CBD in EGI (N613) severely influenced the hydrolytic activity of cellulase on insoluble substrates [30].

3.5. Visualization of endoglucanase binding

Phase data are sensitive to local hydrophilicity differences with the hydrophobic region appearing bright in phase images during the light–force tapping ($A_{sp}/A_0 = 0.7–0.8$) mode in AFM [17,18]. Enzyme particles are in general more hydrophilic than carbohydrates, and therefore may be detectable. The enzyme

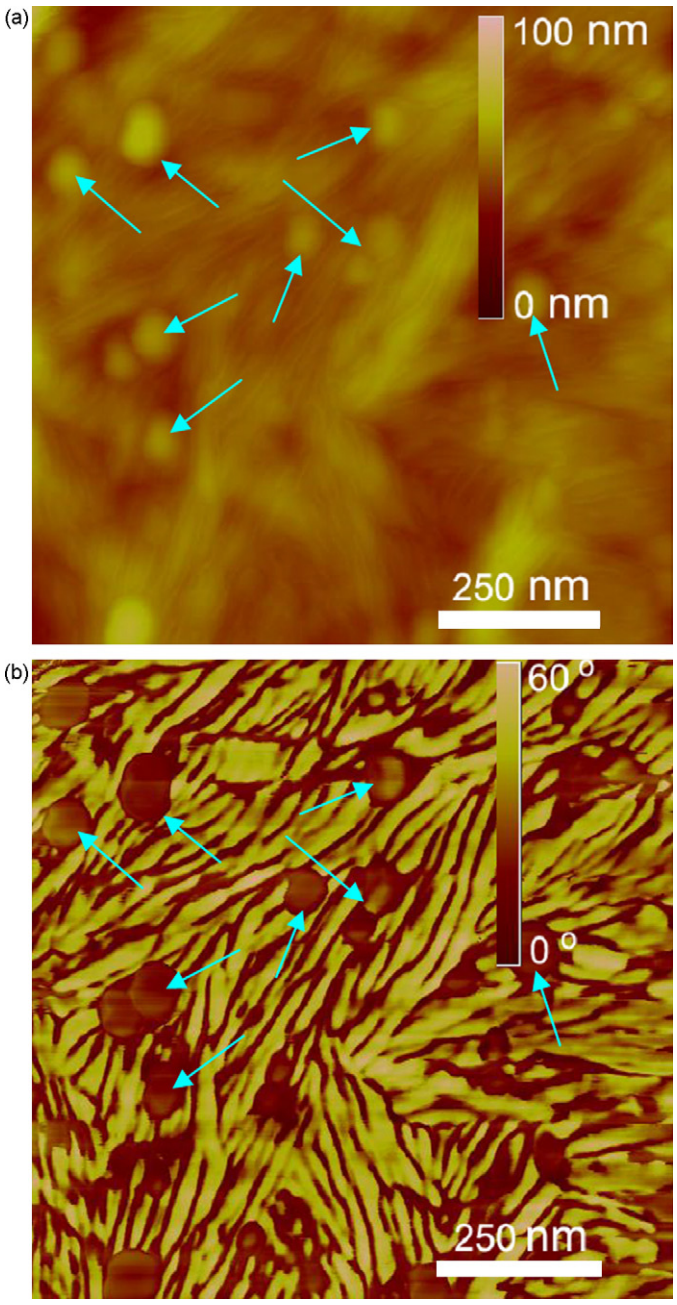

Fig. 7. Atomic force microscopy (AFM) images showing EGV binding onto microfibrils. (a) topographical image; (b) phase image. Some EGV particles are pointed by arrows as examples.

particles of size ranging from 20 to 90 nm, larger than the diameter of microfibrils, can be seen from the sample incubated with EGV for 24 h (Fig. 7a and b). Lee et al. [14] found that the mean grain size of CBH I on cotton fibers was about 13 nm in AFM topographical imaging; furthermore, the CBH I grains appeared to be spherical, which agrees with what we observed from phase imaging (Fig. 7b). Comparing the topographical image (Fig. 7a) to the phase image (Fig. 7b), the advantage of phase imaging over topographical imaging becomes very obvious. The phase image has a much sharper edge of enzyme particles than that shown in the topographical image. The phase of the enzyme particles is around 30°. Moreover, the phase image clearly shows the individual microfibrils with a phase around 50° agree with the peak shown in Fig. 5.

The phase image in Fig. 7b also suggests that it is possible for an aggregated EGV particle to bind to more than one microfibril, perhaps because of the presence of multiple cellulose-binding domains. These binding domains kept enzyme particles in close contact with cellulose substrates [31] and produced specific adsorption sites on cellulose surfaces to enhance the enzyme process. Endoglucanase without CBD, such as EGI (N613) used in this study, can also modify cellulose through catalytic domain [2]. In general, catalytic domain and cellulose-binding domains can work independently [32]. We observed EGI particles aggregated together and covered cellulose surfaces in the form of large patches (not shown due to poor image quality). This unspecific adsorption of EGI may be less effective in modifying cellulose.

4. Conclusions

This study used TM–AFM phase imaging to visualize enzymatic hydrolysis of microfibrils and the binding of enzymes particles on cellulose. The phase images clearly showed the direct actions of cellulases on cellulose to break or modify the ultrastructure of microfibrils. Complete cellulase decomposed microfibrils into fragments in three dimensions, prior to complete solubilization. The AFM phase imaging showed both a down-shift of the low phases and an up-shift of the high phases as the cellulose substrate was degraded and fragmented. The phase shifts can be seen clearly from the phase-bearing area probability density curves calculated from the substrate phase images obtained at different enzyme-incubation time periods. The decrease in high-phase and increase in low-phase bearing area suggests reduction in the covering area of original microfibrils and production of regions of degraded substrate surface through enzymatic hydrolysis. The phase shifts also suggest the increase in the proportion of crystalline regions during hydrolysis, which may be a reason for the decrease in hydrolysis rate. The AFM phase images also show that endoglucanase caused "peeling" action that reduced the diameter of microfibrils but failed to effectively cut down the length, in the so-called "cutting" action, because of the absence of cellobiohydrolases. This study also clearly revealed the binding of individual EGV (with CBD) particles onto microfibrils on cellulose surfaces.

Acknowledgments

We acknowledge the financial support from National High Technology Research and Development Program of China (No. 2007AA100704), the Chinese Scholarship Council and the U.S. Forest Service Program of Biomass, Bioenergy, and Bioproducts (2008) for supporting Mr. Hao Liu's visiting appointment at the U.S. Forest Service, Forest Products Laboratory.

References

[1] Wyman CE. Biomass ethanol: technical progress, opportunities, and commercial challenges. Annual Review of Energy and the Environment 1999;24:189–226.
[2] Lynd LR, Weimer PJ, van Zyl WH, Pretorius IS. Microbial cellulose utilization: fundamentals and biotechnology. Microbiology and Molecular Biology Reviews 2002;66(3):506–77.
[3] Kleman-Leyer KM, SiikaAho M, Teeri TT, Kirk TK. The cellulases endoglucanase I and cellobiohydrolase II of *Trichoderma reesei* act synergistically to solubilize native cotton cellulose but not to decrease its molecular size. Applied and Environmental Microbiology 1996;62(8):2883–7.
[4] Zhang YHP, Himmel ME, Mielenz JR. Outlook for cellulase improvement: screening strategies. Biotechnology Advances 2006;24(7):452–81.
[5] Teeri TT, Koivula A, Linder M, Wohlfahrt G, Divne C, Jones TA. *Trichoderma reesei* cellobiohydrolases: why so efficient on crystalline cellulose? Biochemical Society Transactions 1998;26(2):173–8.
[6] Wood TM, McCrae SI. The cellulase of *Trichoderma koningii*. Purification and properties of some endoglucanase components with special reference to their action on cellulose when acting alone and in synergism with the cellobiohydrolase. Biochemical Journal 1978;171:61–72.
[7] Manley RSJ. Fine structure of native cellulose microfibrils. Nature 1964;204:1155–7.

[8] Fujita M, Harada H. Ultrastructure and formation of wood cell wall. In: Wood and cellulosic chemistry. New York: Marcel Dekker, Inc.; 2000. p. 7–10.
[9] Mühlethaler K. Ultrastructure and formation of plant cell walls. Annual Review of Plant Physiology 1967;18:1–24.
[10] White AR, Brown Jr RM. Enzymatic hydrolysis of cellulose: visual characterization of the process. Proceedings of the National Academy of Sciences of the United States of America 1981;78(2):1047–51.
[11] Paiva AT, Sequeira SM, Evtuguin DV. Nanoscale structure of cellulosic materials: challenges and opportunities for AFM. In: Mendez-Vilas A, Diaz J, editors. Modern research and educational topics in microscopy, formatex microscopy. 2007. p. 726.
[12] Hanley SJ, Giasson J, Revol J-F, Gary DG. Atomic force microscopy of cellulose microfibrils: comparison with transmission electron microscopy. Polymer 1992;33:4639–42.
[13] Howard AJ, Rye RR, Houston JE. Nanomechanical basis for imaging soft materials with tapping mode atomic force microscopy. Journal of Applied Physics 1996;79(4):1885–90.
[14] Lee I, Evans BR, Woodward J. The mechanism of cellulase action on cotton fibers: evidence from atomic force microscopy. Ultramicroscopy 2000;82: 213–21.
[15] Lee I, Evans BR, Lane LM, Woodward J. Substrate-enzyme interactions in cellulase systems. Bioresource Technology 1996;58:163–9.
[16] Tamayo J, Garcia R. Effects of elastic and inelastic interactions on phase contrast images in tapping-mode scanning force microscopy. Applied Physics Letters 1997;71(20):2394–6.
[17] Simola J, Malkavaara P, Alen R, Peltonen J. Scanning probe microscopy of pine and birch kraft pulp fibers. Polymer 2000;41:2121–6.
[18] Brandsch R, Bar G, Whangbo M-H. On the factors affecting the contrast of height and phase images in tapping mode atomic force microscopy. Langmuir 1997;13(24):6349–53.
[19] Chernoff DA. Industrial application of topographic and chemical imaging of polymers. Ploymer Preprints 1996;37(2):599–600.
[20] Donaldson LA. Ultrastructure of wood cellulose substrates during enzymatic hydrolysis. Wood Science and Technology 1988;22:33–41.
[21] Yoshihiko A, Takahisa K. New insights into cellulose degradation by cellulases and related enzymes. Trends in Glycoscience and Glycotechnology 2002;14(75):27–34.
[22] Moran-Mirabal JM, Santhanam N, Corgie SC, Carighead HG, Walker LP. Immobilization of cellulose fibrils on solid substrates for cellulase-binding studies through quantitative fluorescence microscopy. Biotechnology and Bioengineering 2008;101(6):1129–41.
[23] Fu SY, Chu QF, Zhan HY. Degradation of residual lignin of reed kraft pulp by laccase and mediator system. China Pulp and Paper 2001;118:17–20.
[24] Zhan HY, Yue BZ, Hu WJ, Huang WF. Kraft reed pulp TCF bleaching with enzyme pretreatment. Cellulose Chemistry and Technology 1999;33(1-2):53–60.
[25] TAPPI. Tappi Test Methods, TAPPI, Atlanta, 1997, T-236, T-230, T-525.
[26] Ghose TK. Measurement of cellulase activities. Pure and Applied Chemistry 1987;59:257–68.
[27] Miller GL. Use of dinitrosalicylic acid reagent for determination of reducing sugar. Analytical Chemistry 1959;31:426–8.
[28] Köpcke V. Improvement on cellulose accessibility and reactivity of different wood pulps. Ph.D. dissertation. Stockholm, Sweden: Royal Institute of Technology; 2008. p. 18–19.
[29] Gilkes NR, Henrissat B, Kilbum DG, Miller Jr KC, Warren RAJ. Domains in microbial beta-1, 4-glycanases: sequence conservation, function, and enzyme families. Microbiology and Molecular Biology Reviews 1991;55(2):303–15.
[30] Linder M, Teeri TT. The roles and function of cellulose-binding domains. Journal of Biotechnology 1997;57(1-3):15–28.
[31] Kormos J, Johnson PE, Brun E, Tomme P, McIntosh LP, Haynes CA, et al. Binding site analysis of cellulose binding domain CBD(N1) from endoglucanse C of *Cellulomonas fimi* by site-directed mutagenesis. Biochemistry 2000;39(30):8844–52.
[32] Arai T, Araki R, Tanaka A, Karita S, Kimura T, Sakka K, et al. Characterization of a cellulase containing a family 30 carbohydrate-binding module (CBM) derived from *Clostridium thermocellum* cell: importance of the CBM to cellulose hydrolysis. Journal of Bacteriology 2003;185(2):504–12.